

Optimization of slow and stored light in atomic vapor

Irina Novikova^{a,b}, Alexey V. Gorshkov^c, David F. Phillips^a, Yanhong Xiao^a, Mason Klein^{a,c},
Ronald L. Walsworth^{a,c}

^aHarvard-Smithsonian Center for Astrophysics, Cambridge, MA, 02138 USA

^bDepartment of Physics, College of William & Mary, Williamsburg, VA 23185, USA

^cDepartment of Physics, Harvard University, Cambridge, MA, 02138 USA

ABSTRACT

We present a preliminary experimental study of optimized slow and stored light pulses in Rb vapor cells. We study the efficiency of light storage as a function of pulse duration, storage time, retrieval field intensity, etc. We demonstrate a procedure based on time reversal for the optimization of the efficiency for storage of light in atomic ensembles suggested in a recent theoretical paper [A.V. Gorshkov *et al.*, e-print archive quant-ph/0604037 (2006)]. Experimental results are in a good qualitative agreement with theoretical calculations based on a simplified three-level model.

Keywords: Electromagnetically induced transparency, slow light, stored light, vapor cell, buffer gas

1. INTRODUCTION

Experimental realization of a quantum memory for photons is important for many applications, including quantum repeaters,^{1,2} entanglement purification, and many quantum cryptography protocols.³⁻⁶ One promising approach to realizing a quantum memory is based on the coherent and reversible transfer of quantum states of photons to long-lived quantum states of individual atoms or ions, or to a collective excitation of many atoms.⁷ The latter case is of particular interest because of its potential scalability.

In a quantum memory based on ultra-slow light pulse propagation under conditions of electromagnetically induced transparency (EIT),^{8,9} a strong, classical, “control” field determines the group velocity of a weak (classical or quantum) “signal” field through a resonant atomic medium in a Λ configuration shown in Fig. 1. The control field creates a strong coupling between signal field photons and the collective excitation of atomic spins. The group velocity, v_g , for the signal pulse is

$$v_g = \frac{c}{1 + g^2 N / |\Omega|^2}, \quad (1)$$

where N is the number of atoms, g the atom-field coupling coefficient, Ω the control field Rabi frequency, $|\Omega|^2 = \wp_{es}^2 I / (2\hbar^2 \epsilon_0 c)$, where \wp_{es} is the dipole moment of the optical transition, c , the speed of light, and I the control field intensity. By reducing the control field intensity to zero, the group velocity is also reduced to zero and the photonic excitation is coherently mapped into a spin wave. Ideally, this process is completely reversible, *i.e.*, the original photons can be recreated by turning the control field back on. This “stored light” process has been experimentally demonstrated in proof-of-principle experiments for both classical pulses^{10,11} and few-photon, non-classical pulses.^{12,13}

An effective quantum memory requires high efficiency light storage. Here, efficiency is the probability of retrieving an input photon after storing it in an atomic ensemble. In practice, this efficiency is reduced by many factors including spin wave dephasing and residual incoherent absorption of the input pulse. Even under idealized conditions of negligible spin decoherence there is a fundamental limit on storage efficiency due to the finite optical depth of an atomic medium¹⁴ with completely reversible mapping of a photonic state to a collective atomic spin state possible only in the limit of infinite optical depth.^{7,14} While the maximum storage efficiency depends only on the optical depth (with losses scaling as the inverse of the optical depth) and the propagation direction of the control field during the writing and retrieval stages,¹⁵ and not on the details of the control field shape,¹⁷ the maximum efficiency is achieved only if the temporal profiles of control and signal pulses are mutually optimized for given optical depth.^{14,15}

Lossless storage is only possible for small group velocity and large EIT bandwidth. The group velocity must be low enough that the entire pulse resides in the atomic medium when the control field is reduced to zero (*i.e.* $L/v_g < \tau_{pulse}$, where L is the vapor cell length, and τ_{pulse} is the pulse duration). The spectral bandwidth of the pulse, must also be less than the EIT bandwidth, $\tau_{pulse}\gamma_{EIT} \ll 1$, to avoid pulse absorption and reshaping.

In a three-level Λ -system, the EIT width, γ_{EIT} , is:⁹

$$\gamma_{EIT} = \frac{|\Omega|^2}{\sqrt{\gamma g^2 N k L}}, \quad (2)$$

where $k = 2\pi/\lambda$ is the wave vector, γ_0 and γ are relaxation rates of the ground-state and optical coherences respectively, and we assume the power-broadened EIT limit $|\Omega|^2 \gg \gamma_0\gamma$. Both the group velocity (Eq. [1]) and the EIT bandwidth (Eq. [2]) are proportional to the square of the control field Rabi frequency. Therefore, it is impossible to satisfy both the condition on the group velocity and the EIT bandwidth by changing only the control field for a fixed optical depth.

Here we study experimentally the optimization of both the control field and the shape of an input signal pulse to minimize the effects of spin decoherence and absorption. We demonstrate the light storage optimization procedure to find the temporal profile of a signal field pulse which is stored and retrieved with maximum efficiency. We confirm that for a given control pulse the optimization procedure results in a unique signal field pulse shape independently of the initial signal field settings. Finally, we test that while different control field profiles result in different optimal signal pulse shapes, they yield the same optimized efficiency, as the theory predicts.¹⁴ We also obtain qualitative agreement between the experimental results observed here and a theoretical model with no adjustable parameters.

2. OPTIMIZATION PROCEDURE

The optimal storage process is time-reversible, *i.e.*, the retrieval stage is the same as the writing stage with time reversed.¹⁴ The optimal signal pulse can be found experimentally using an iteration optimization method. The initial optimization step consists of the storage of an arbitrary signal pulse with chosen control field profile into an atomic spin wave followed by pulse retrieval using a control field that is the time-reverse of the writing control field. The measured retrieved signal pulse becomes the input pulse for the next iteration step, and so on. After several iterations the signal pulse shape converges to the optimized temporal profile. Time reversal during the retrieval procedure requires backward retrieval – the retrieval control field must propagate in the opposite direction to the writing control field. For a degenerate Λ -scheme, this method also provides maximum storage efficiency.¹⁴

For non-degenerate Λ -systems, backwards-retrieval leads to reduced efficiency¹⁵ due to transfer of momentum from the laser fields to the spin wave during light storage. Therefore, in the experiments described here we use stored light with forward retrieval (*i.e.*, the write and retrieval control pulses propagate in the same direction). In this case the optimization procedure is more complicated, since the write and retrieval control fields cannot be a pair of time-reversed fields (as they co-propagate). Time-reversible optimization of writing followed by forward retrieval requires two write and retrieval cycles.¹⁵ First, an input pulse is stored and then retrieved using independent co-propagating control fields for the writing stage (first control field) and for the retrieval stage (second control field). The process is then time-reversed: the read-out signal pulse is stored using the second control field and retrieved using the first control field. The resulting pulse becomes the input pulse for the next cycle. We simplify this process, reducing the number of steps, by spatially reversing the second half of the process and identifying the retrieval control field and the time- and space-reversed writing control field; similarly the optimal retrieved signal pulse is the time- and space-reverse of input signal pulse shape. In this simplified process, the second (time-reversed) storage and retrieval cycle is identical to the first, yielding the experimental optimization procedure described below. The iteration procedure used in this experiment is illustrated in Fig. 1. Each iteration step includes two parts. First, in the writing stage, an input signal pulse is stored as a spin wave in the atomic ensemble. Then, during the retrieval stage, the spin wave is retrieved using a retrieval control field that is identical to the time-reversed writing control field, propagating in the same direction. The retrieved pulse

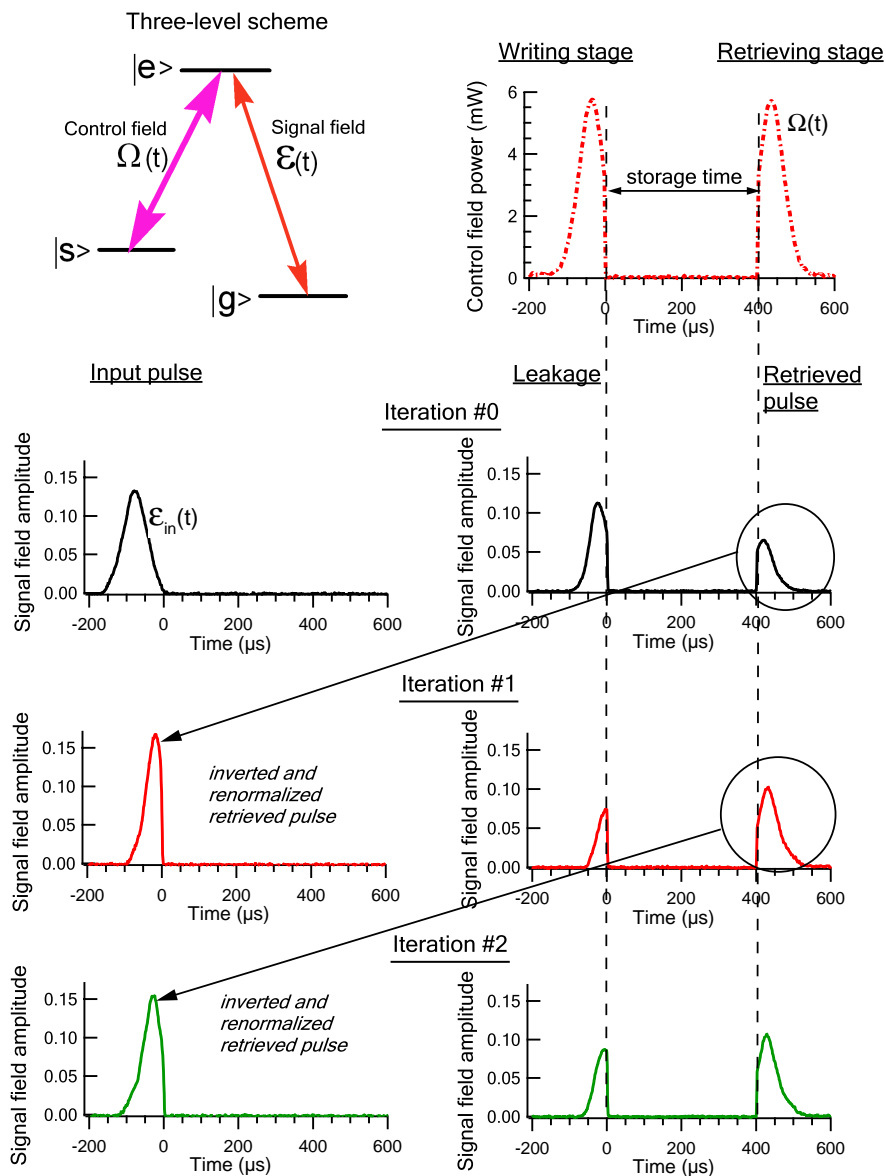


Figure 1. Schematic of the optimization procedure. Upper left: idealized interaction scheme showing relevant atomic levels and control and signal fields. Upper right: control fields during storage and retrieval process. Lower three rows: input signal pulses during three iterations of the optimization process in the left column with the initial input pulse in the first row and the pulses derived from the previous iteration's output pulse in the following rows. Signal field leakage during the write process and the retrieved pulse are shown on the right. Signal pulses are normalized such that the integrated power of the input signal pulse is one for time measured in μs . (See text for details.)

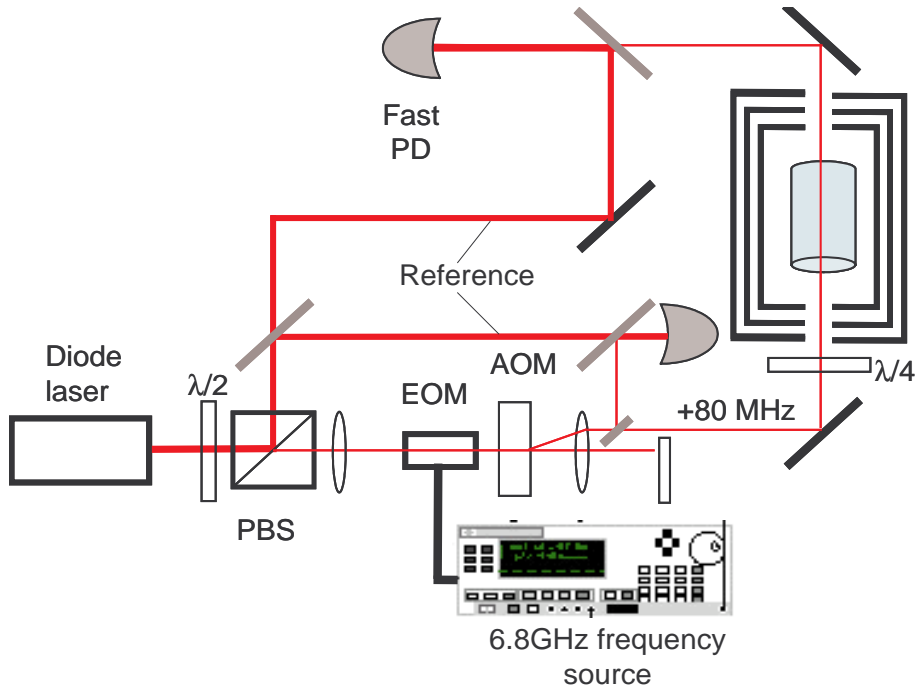


Figure 2. Experimental setup. All optical fields are derived from a single diode laser. The signal field is generated from the laser field using an electro-optical modulator (EOM), and the total laser power is varied using an acousto-optic modulator (AOM), which simultaneously shifts frequencies of both control and signal fields by 80 MHz. Both the input and output signal pulses are measured as the beatnote signal between a signal field and an unmodulated reference field from the diode laser using fast photo-detectors. The vapor cell is surrounded by high-permeability magnetic shields, which screen out external magnetic fields. (See text for details.)

is then measured on a photodetector and the output pulse shape is used to determine the new signal pulse for the next writing stage.

We tested the iteration procedure using weak classical signal pulses. Since the theoretical analysis¹⁴ applies equally well to quantized and to weak classical signal fields, conclusions from the study of classical pulses could be applied to the quantized regime. For weak, classical pulses we defined the efficiency as the energy of the retrieved signal pulse divided by the energy of the input pulse, and we tested that the efficiency grows with each iteration until convergence. We started with the storage of a Gaussian profile signal field (Fig. 1: iteration #0). Because the group velocity in the medium was larger than the length of the atomic medium divided by the temporal length of the pulse, a large fraction of the input signal pulse escaped the cell before the control field was turned off. However, some of the pulse was stored as an atomic spin wave (iteration #0, writing stage). After a 400 μs storage interval, we turned on the time-reversed control field (iteration #0, retrieve stage), and detected the retrieved signal pulse. We then digitally reversed and normalized the detected pulse shape to unit pulse energy and used it as an input pulse for iteration #1. To find the optimal input pulse shape, we repeated these steps several times until the shape of the retrieved pulse was identical to the reversed profile of the input pulse (though the amplitude of the retrieved pulse was attenuated because of imperfect efficiency). The resulting pulse shape provided the highest efficiency of storage at the given control field (and fixed optical depth).

3. EXPERIMENTAL SETUP

We tested the optimization procedure described above using the experimental setup shown in Fig. 2. We phase-modulated the output of an external-cavity diode laser using an electro-optical modulator (EOM) at a frequency equal to the ground state hyperfine splitting in ^{87}Rb (6.835 GHz). The unmodulated laser frequency was tuned to the $5^2\text{S}_{1/2}, F = 2 \rightarrow 5^2\text{P}_{1/2}, F' = 2$ transition and served as the control field, and a high-frequency

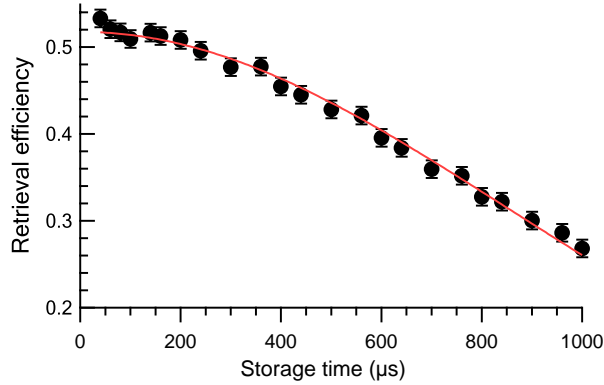


Figure 3. Storage efficiency as a function of the storage time. The solid line is a smooth curve to guide the eye. The time at which the efficiency has dropped to $1/e$ of its short-time value is slightly longer than 1 ms.

modulation sideband, resonant with the $5^2S_{1/2}, F = 1 \rightarrow 5^2P_{1/2}, F' = 2$ transition, served as the signal field. For experimental realization of the iteration procedure we controlled the amplitudes of both the signal and control fields independently. An acousto-optical modulator (AOM) controlled the total laser power and thus the control field, and also shifted the frequency of all optical fields by 80 MHz. The EOM modulation amplitude was then adjusted to compensate for changes in signal field intensity due to total laser intensity variations. The laser beam was collimated to a 6.8 mm diameter spot and circularly polarized using a quarter-wave plate ($\lambda/4$) before entering a cylindrical 7.5 cm-long glass cell, containing isotopically enriched ^{87}Rb and 40 Torr of Ne buffer gas. This buffer gas pressure leads to a rubidium diffusion coefficient of $4 \text{ cm}^2/\text{s}$ and a lowest order diffusion time constant of rubidium atoms out of the laser beam of 7 ms. (Note that for this large buffer gas pressure and laser beam diameter repeated diffusion of atomic coherence in and out of the laser beam¹⁸ is a small effect.) The vapor cell was mounted inside a three-layer magnetic shield, which reduced stray magnetic fields. Unless otherwise specified, the temperature of the cell was 60°C .

After the cell, the transmitted light was mixed with a reference beam at the unmodulated laser frequency (see Fig. 2), and the beatnote between the signal field and the reference field was detected using a fast photodiode. Mixing the transmitted light with the unmodulated field and using frequency-selective detection after the fast photo detector ensured that only the signal field amplitude was detected. To measure the input pulse shape we split the beam before the cell and sent it to a detection system analogous to the one after the cell.

We define the efficiency of light storage as the ratio between the energies of the retrieved and input pulses, excluding all technical losses due to, *e.g.*, imperfect fiber coupling, unwanted reflections, limited photodetector quantum efficiency, etc. To estimate optical losses not associated with atoms we measure the transmission of a far-detuned ($\approx +4 \text{ GHz}$) signal field through our optical system, and normalize all pulses to that value. The energy of a pulse is calculated as the integral of its squared amplitude, since the measured beatnote power is proportional to the signal field amplitude. When plotting signal pulses we normalize them such that the energy of all input pulses is equal to one for time measured in μs . The retrieved pulse energy is then equal to storage efficiency and can be estimated directly from the graphs.

We measure atomic losses in our system by varying the storage time, as shown in Fig. 3. Observed efficiency decays to $1/e$ of its initial value in slightly over 1 ms. For storage times of $400 \mu\text{s}$ used throughout the experiments reported here, only 10% of the initially stored spin wave decays during the storage interval. As discussed above, the timescale associated with the lowest order diffusion mode is approximately 7 ms and thus plays a negligible role in spin wave decoherence. We expect that residual magnetic fields are the dominant source of decoherence in our system.

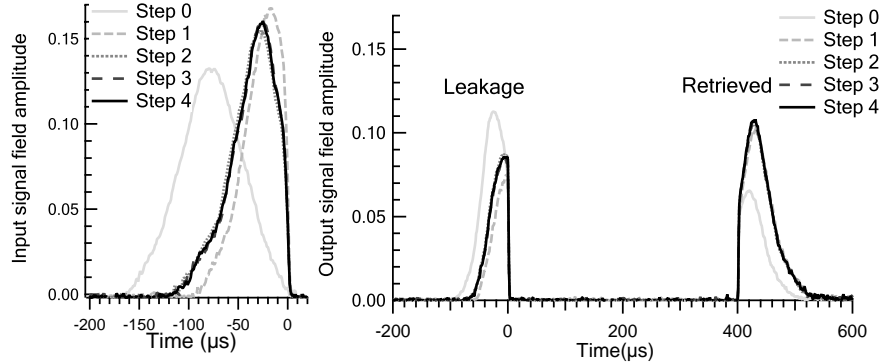


Figure 4. Input pulses (left) and storage and retrieval sequences (right) for the experimental optimization procedure. The initial signal pulse shape is a Gaussian profile with FWHM = 77 μs , maximum at -81 μs . Control field power is shown in Fig. 1.

4. EXPERIMENTAL RESULTS

Signal pulse shapes rapidly converged in our optimization process, as shown when all iterations of Fig. 1, were combined in Fig. 4. After a few iterations the signal pulse shape converged to a particular profile, and the retrieved signal pulse shape was the attenuated mirror image of the input pulse. The efficiency of the retrieval grew with every iteration until saturating at its maximum value, as estimated from the area of the retrieved pulses (see also Fig. 5a).

The success of the optimization procedure should not depend on the initial signal pulse.¹⁴ Therefore, we compared the results of the procedure with several initial input pulses which all converged to the same pulse shape after 2-3 iterations (see Fig. 5a). The efficiency reached the same maximum level, even though the pulse shapes and efficiencies for the first few storage and retrieval steps differed. Using a control field with a different shape (the flat control field of Fig. 5b), we confirmed the properties of the optimization procedure did not depend upon the details of the control field. For the flat control field, the optimized pulse shape again did not depend upon the initial input pulse. Additionally, the same storage efficiency was achieved for both control fields as a result of optimization procedure.

To further test the independence of the achievable storage efficiency on the control field parameters, we measured the optimal storage efficiency for a variety of control fields, varying both the shape and overall amplitude (Fig. 6). During retrieval, we used the reversed temporal profile of the writing control field, as described in the optimization algorithm (Sec. 2). For each control field considered (Fig. 6a-d), we confirmed that the input signal pulse shapes converged to the same profile independent of the initial input pulse. We also confirmed that the iteration procedure converged to a unique optimized signal pulse shape (Fig. 6a-d) for each control field. The maximum measured storage efficiency was also independent of the details of the control field as shown in Fig. 6e. Since high control field power resulted in short signal pulses, large enough control field power was used to keep the duration of the signal pulses shorter than the characteristic decay time of the spin wave decay to avoid the effect of spin wave decoherence during writing and retrieval stages. We observed experimentally and confirmed theoretically that if pulse duration was comparable with the spin wave decay time, storage efficiency was reduced. We, thus, confirmed the theoretical prediction that for negligible spin wave decay during the writing and retrieval stages the optimal efficiency does not depend on the control field.

5. THEORETICAL CALCULATIONS

To confirm that the experimental results obtained with a weak classical signal field can be directly related to the light storage of a few-photon non-classical pulse we compare the experimental results with theoretical calculations for a fully-quantized signal field. To model the stored light optimization procedure, we approximate Rb atoms using a three-level system, shown in Fig. 1. We perform calculations in two approximations. The first,

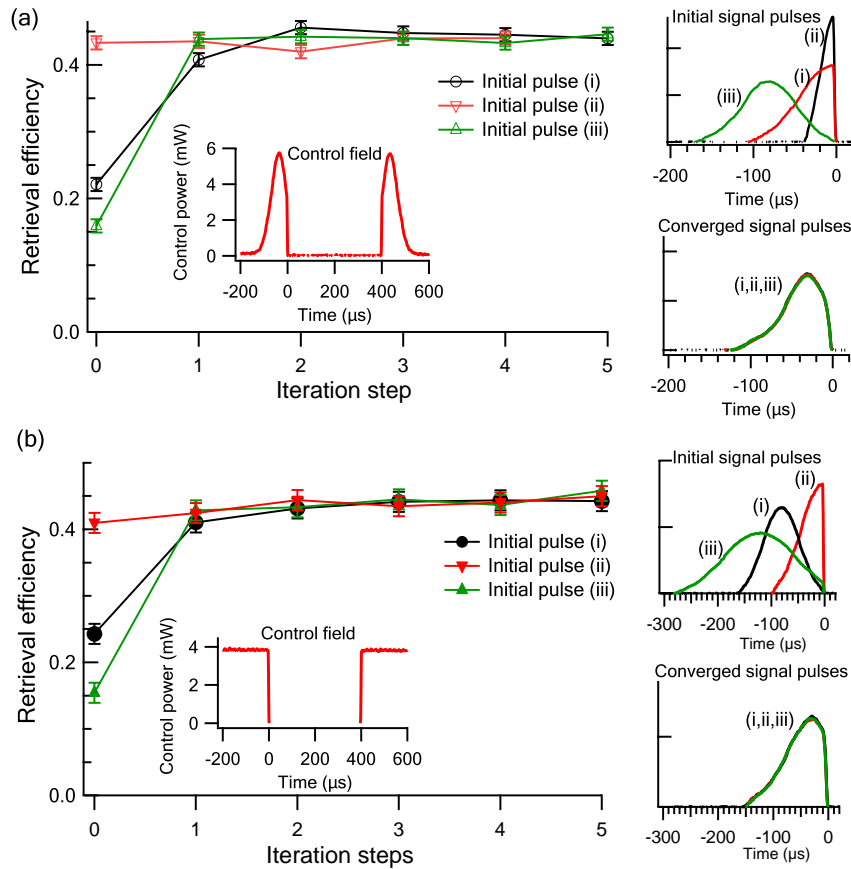


Figure 5. (a) Measured efficiency vs. iteration (left) for different initial input pulses (shown on top-right graph). The second graph on the right shows converged signal pulses (after 5 iterations) for each pulse shape. The control field is shown in the inset and is the same as in the previous figures. (b) Same as (a) but for a flat control field (control field power is a constant 3.8 mW during storage and retrieval stages).

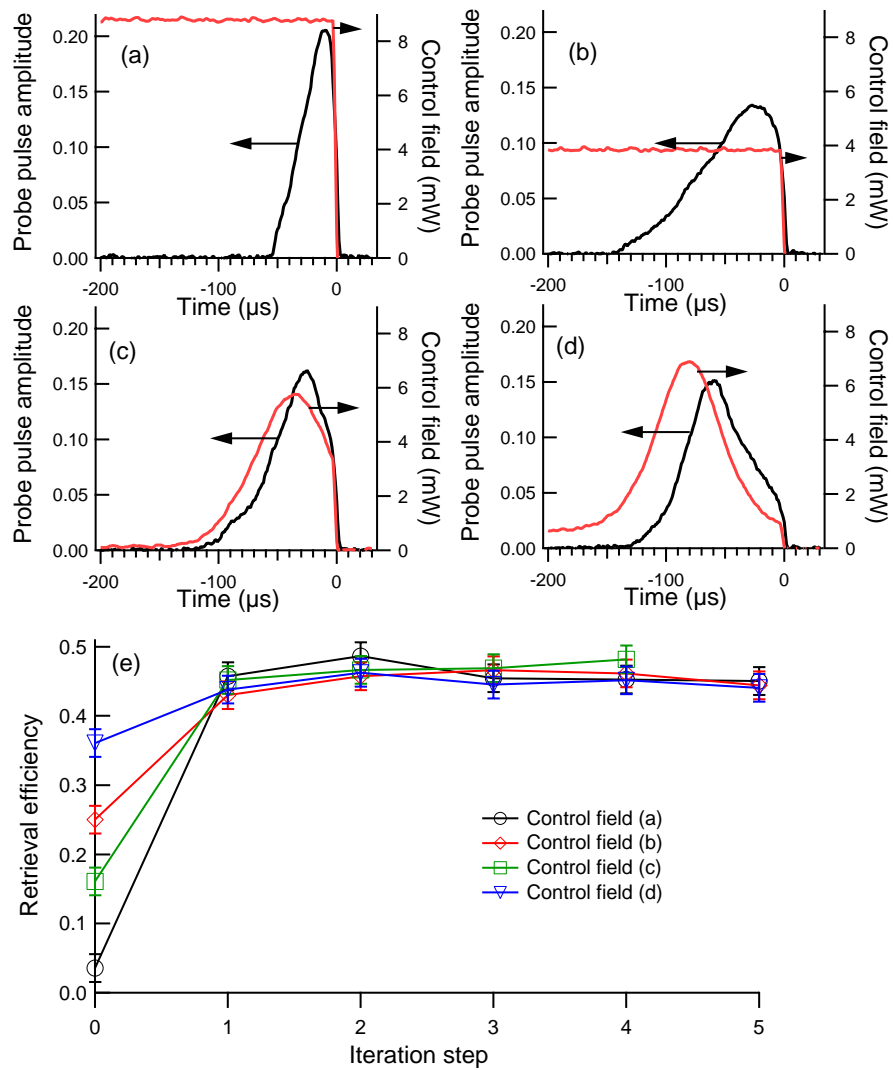


Figure 6. (a)-(d) Optimal signal input pulses (units as in Fig. 4) for different control field profiles. In all cases, the initial input has the same Gaussian profile (FWHM = 77 μs , maximum at -81 μs). (e) Experimentally measured efficiencies as functions of the iteration cycle number. For all control fields, the optimal efficiency is the same.

labeled “simple theory,” ignores Doppler broadening of the optical transitions and velocity-changing collisions of Rb atoms. This is a reasonable assumption under the experiment’s conditions, since the pressure broadened homogeneous width of the optical transition $\gamma = (2\pi)200$ MHz is comparable with the Doppler width at 60°C $\gamma_D = (2\pi)264$ MHz.

In this case, the propagation of a signal pulse is described by three variables:¹⁴ \mathcal{E} , the slowly-varying envelope for the signal field; P , the optical polarization of the $|g\rangle - |e\rangle$ transition; and S , the spin wave coherence. The equations of motion are

$$(\partial_t + c\partial_z)\mathcal{E}(z, t) = ig\sqrt{N}P(z, t) \quad (3)$$

$$\begin{aligned} \partial_t P(z, t) &= -\gamma P(z, t) + ig\sqrt{N}\mathcal{E}(z, t) + \\ &\quad i\Omega(t - z/c)S(z, t) \end{aligned} \quad (4)$$

$$\partial_t S(z, t) = -\gamma_0 S(z, t) + i\Omega(t - z/c)P(z, t), \quad (5)$$

with $\Omega(t)$ the time-varying control field Rabi frequency, g the single-atom coupling constant, N the atomic density, γ_0 the ground-state relaxation rate, γ the homogeneously broadened optical coherence decay rate, and c the speed of light. We assume negligible losses for the control field. The experiment was performed in the adiabatic limit,¹⁴ in which $\partial_t P \ll \gamma P$. In this limit, the equations can be solved analytically by adiabatically eliminating P .

To make connection between theory and experiment, we accounted for the full 16-level structure of the D_1 line of ^{87}Rb atoms in our three-level Λ -system model. We calculated the effective control-field Rabi frequency and optical depth,¹⁶ d . Once we determined the optical depth we found the coupling constant $g\sqrt{N} = \sqrt{\gamma cd/L}$ for the signal field, with L the length of the atomic medium. The ground-state population distribution in a 16-level ^{87}Rb atom after optical pumping depends on the population-transfer rates between the eight excited-state sublevels due to collisions with neon^{19,20} at the corresponding depolarization rate $\gamma_{\text{depol}} = (2\pi)255$ MHz,²¹ as well as the pressure broadening and the Doppler broadening. We found that the population transfer between excited state sublevels at 40 Torr Ne is fast enough to ensure roughly equal (25%) population in each of the $(F, m_F) = (1, -1), (1, 0), (1, 1),$ and $(2, 2)$ ground state sublevels. Using the pressure broadened linewidth of $2\gamma = (2\pi)390$ MHz,²² we then calculate optical depth d as a function of Rb number density and find, for example, that at 60°C (Rb vapor density of $2.5 \times 10^{11} \text{ cm}^{-3}$) the optical depth is $d = 9.0$. Due to a large Clebsch-Gordon coefficient, $\approx 60\%$ of this optical depth came from $(F, m_F) = (1, 1)$. Therefore, to approximate control field Rabi frequency Ω , we use the dipole matrix element of the $|F = 2, m_F = 1\rangle \rightarrow |F' = 2, m_F = 2\rangle$ transition. For simplicity, we approximate the laser beam with the Gaussian transverse profile with a uniform cylindrical beam of diameter 6.8 mm; in this case we find, for example, that for the laser power of 3.8 mW the corresponding Rabi frequency is $\Omega = (2\pi)2.2$ MHz. This derivation of d and Ω and the remainder of the theoretical modelling are performed with no free parameters, yet it provides good agreement with the experimental results, as discussed below.

We also performed the same calculations in a more realistic approximation, taking into account inhomogeneous Doppler broadening of Rb atoms and velocity changing collisions with buffer gas atoms. We used the simplest collisional kernel²³ with the calculated rate of $(2\pi)15$ MHz for completely thermalizing collisions. Such calculations were performed numerically and are labeled “complete theory” (to distinguish from the “simple theory”). However, the “complete” theory is still a simplified model of the actual interaction process which does not fully take into account the multilevel structure of the ^{87}Rb D_1 line, the inhomogeneous transverse profile of the control field, four-wave mixing processes,²⁴ and three-dimensional effects.²⁵

The results of the theoretical simulations of the iterative optimization process are shown in rows two and three of Fig. 7 for the “simple” and “complete” theories, respectively. With both models, the calculated pulse shapes are qualitatively similar to the experimental results and converge to the optimal pulse shapes within a few iteration steps. The “complete” theory provides convergence rates and the pulse shapes that are slightly closer to the experimental results than the “simple” theory. Yet even the “simple” theory qualitatively reproduces the experimental results. The calculated efficiencies for the optimization process are shown in Fig. 8. Although the efficiencies predicted by the theory are lower than the experimentally observed efficiencies, both the calculated and the experimental efficiencies take about the same number of steps (two to three) to converge.

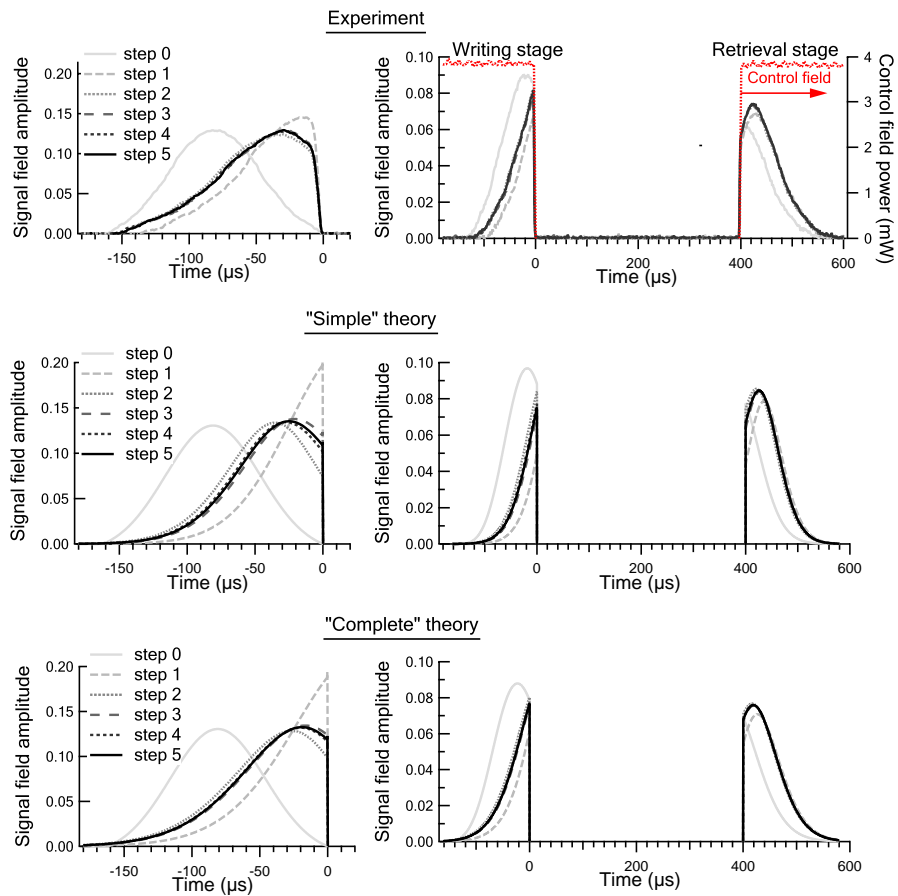


Figure 7. Input pulses (left) and storage and retrieval sequences (right) for each iteration of the optimization procedure. The initial input pulse (step 0) was chosen as a Gaussian pulse with FWHM = 77 μs and maximum at $t = -81 \mu\text{s}$. The area under the squared amplitude of each input pulse is normalized to one. Control field power is constant (3.8 mW) during both storage and retrieval stages (the measured control field is shown in the top right graph). The top row is experimental data, and rows two and three show calculations based on “simple” and “complete” theoretical models, respectively. (See text for the details.)

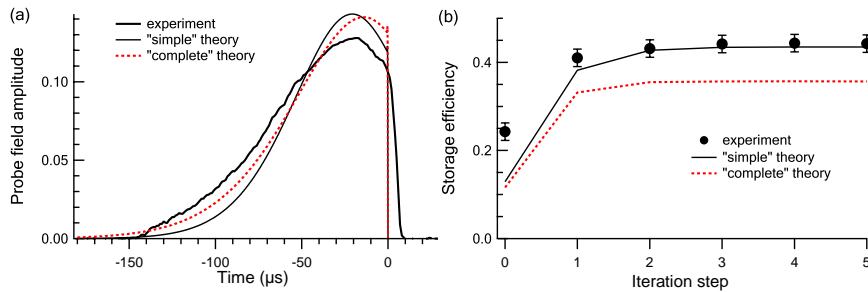


Figure 8. (a) Comparison of optimal experimental signal field pulse shape and those calculated under two different approximations. (b) Comparison of experimental and theoretical efficiencies of light storage as functions of iteration. All experimental conditions are the same as in Fig. 7.

6. CONCLUSIONS

We experimentally demonstrated a powerful time-reversal-based optimization procedure that allows one to iteratively find the pulse shape of a weak input field that maximizes the efficiency of light storage and retrieval, confirming the prediction that the optimal efficiency does not depend on the control field temporal profile.^{14,15} Theoretical calculations with no free parameters showed good qualitative agreement with the experimental results, thus, confirming the validity of our interpretation. Since the analysis is applicable to both classical and quantum signal fields,^{14,15} the conclusions of our classical experiments strongly indicate the validity of such an optimization procedure in the quantum, e.g. single-photon, regime, as well. Moreover, the classical light storage optimization demonstrated in the present work can be directly used as a tool for quantum light storage optimization: the easily accessible iterations with classical light can be used to find optimal input pulse shapes, which can then be used to choose the optimal temporal profile for the quantum fields, for which the iterations rely on mode shape measurement and generation that are much harder to carry out.

We are grateful to M. Hohensee and A. S. Sørensen for useful discussions. This work was supported by ONR, DARPA, NSF, and the Smithsonian Institution.

REFERENCES

1. H.-J. Briegel, W. Dur, J. I. Cirac, and P. Zoller, Phys. Rev. Lett. **81**, 5932 (1998).
2. H. J. Briegel, W. Dur, S. J. van Enk, J. I. Cirac, and P. Zoller in *The Physics of Quantum Information* (eds D. Bouwmeester, A. Ekert, and A. Zeilinger) 281-293 (Springer, Berlin, 2000).
3. L. M. Duan, M. D. Lukin, J. I. Cirac, and P. Zoller, Nature **414**, 413 (2001).
4. A. K. Ekert, Phys. Rev. Lett. **67**, 661 (1991).
5. E. Knill, and R. Laflamme, Phys. Rev. A **55**, 900 (1997).
6. M. Hillery, V. Bužek, and A. Berthiaume, Phys. Rev. A **59**, 1829 (1999).
7. M. D. Lukin, Rev. Mod. Phys. **75**, 457 (2003).
8. S. E. Harris, Phys. Today **50** (7), 36 (1997).
9. M. O. Scully, and M. S. Zubairy, *Quantum Optics* (Cambridge University Press, Cambridge, UK, 1997).
10. C. Liu, Z. Dutton, C. H. Behroozi, and L. V. Hau, Nature **409**, 490 (2001)
11. D. F. Phillips, A. Fleischhauer, A. Mair, R. L. Walsworth, and M. D. Lukin, Phys. Rev. Lett. **86**, 783 (2001); A. Mair, J. Hager, D. F. Phillips, R. L. Walsworth, and M. D. Lukin, Phys. Rev. A **65**, 031802 (2002).
12. M. D. Eisaman, A. André, F. Massou, M. Fleischhauer, A. S. Zibrov, and M. D. Lukin, Nature **438**, 837 (2005).
13. T. Chanelière, D. Matsukevich, S. D. Jenkins, S.-Y. Lan, T. A. B. Kennedy, and A. Kuzmich, Nature **438**, 833 (2005).
14. A. V. Gorshkov, A. André, M. Fleischhauer, A. S. Sørensen, and M. D. Lukin, e-print archive quant-ph/0604037 (2006).
15. A.V. Gorshkov, A. André, M. Fleischhauer, A. S. Sørensen, and M. D. Lukin, e-print archive quant-ph/0612083(2006).
16. We define optical depth d as an amplitude attenuation of a weak resonant signal pulse with no control field; the intensity attenuation is given by $\exp(-2d)$.
17. This statement assumes negligible spin wave decay and sufficiently large control pulse energy ($\int dt \Omega^2 \gg \gamma d$ where 2γ is the linewidth).
18. Y. Xiao, I. Novikova, D. F. Phillips, and R. L. Walsworth, Phys. Rev. Lett. **96**, 043601 (2006).
19. W. Happer, Rev. Mod. Phys. **44**, 169 (1972).
20. F. A. Franz and J. R. Franz, Phys. Rev. **148**, 82 (1966).
21. M. D. Rotondaro and G. P. Perram, Phys. Rev. A **58**, 2023 (1998).
22. M. D. Rotondaro, and G. P. Perram, J. Quant. Spectrosc. Radiat. Transfer **57**, 497 (1997).
23. M. Erhard and H. Helm, Phys. Rev. A **63**, 043813 (2001).
24. G. S. Agarwal, T. N. Dey, and D. J. Gauthier, Phys. Rev. A **74**, 043805 (2006).
25. L.-M. Duan, J. I. Cirac, and P. Zoller, Phys. Rev. A **66**, 023818 (2002).